Applications of Highly-Nonlinear Chalcogenide Glass Devices Tailored for High-Speed All-Optical Signal Processing

Mark D. Pelusi, *Member, IEEE*, Vahid G. Ta'eed, Libin Fu, Eric Mägi, Michael R. E. Lamont, *Student Member, IEEE*, Steve Madden, Duk-Yong Choi, Douglas A. P. Bulla, Barry Luther-Davies, *Senior Member, IEEE*, and Benjamin J. Eggleton, *Senior Member, IEEE*

(Invited Paper)

***Abstract*—Ultrahigh nonlinear tapered fiber and planar rib Chalcogenide waveguides have been developed to enable high-speed all-optical signal processing in compact, low-loss optical devices through the use of four-wave mixing (FWM) and cross-phase modulation (XPM) via the ultra fast Kerr effect. Tapering a commercial As_2Se_3 fiber is shown to reduce its effective core area and enhance the Kerr nonlinearity thereby enabling XPM wavelength conversion of a 40 Gb/s signal in a shorter 16-cm length device that allows a broader wavelength tuning range due to its smaller net chromatic dispersion. Progress toward photonic chip-scale devices is shown by fabricating As_2S_3 planar rib waveguides exhibiting nonlinearity up to $2080\ \mathrm{W}^{-1}\cdot\mathrm{km}^{-1}$ and losses as low as 0.05 dB/cm. The material's high refractive index, ensuring more robust confinement of the optical mode, permits a more compact serpentine-shaped rib waveguide of 22.5 cm length on a 7-cm-size chip, which is successfully applied to broadband wavelength conversion of 40–80 Gb/s signals by XPM. A shorter 5-cm length planar waveguide proves most effective for all-optical time-division demultiplexing of a 160 Gb/s signal by FWM and analysis shows its length is near optimum for maximizing FWM in consideration of its dispersion and loss.**

***Index Terms*—Nonlinear optics, optical planar waveguides, optical propagation in nonlinear media, optical signal processing, optical waveguides.**

I. Introduction

NONLINEAR optical phenomena are exploitable in a variety of forms to enable a suite of all-optical signal processing functions that may play a role in future high-speed and high-capacity optical communication networks. These include signal regeneration [1], [2], time-division demultiplexing [3]–[11], wavelength conversion [12]–[19], phase conjugated/midspan spectrally inverted transmission [20], [21], parametric amplification [22], buffering [23], and logic gating and switching [24], [25]. The all-optical nonlinear approach conveniently avoids the need for optical to electronic conversions, and therefore, circumvents the bandwidth limitations, prohibitive cost, and manufacturing complexity of high-speed optoelectronics. This grows more important as data modulation rates increase beyond the fastest 40 Gb/s systems in service today toward 160-Gb/s serial transmission.

Nonlinear signal processing has previously been performed in various media such as optical fiber [2]–[6], [8], [9], [12], [13], [17], [20], [22], [25], semiconductor optical amplifiers (SOA) [11], [14], [24], and periodically poled $LiNbO_3$ (PPLN) [7]. While speed of SOAs is ultimately limited by carrier recovery effects, optical fiber exploiting the $\chi^{(3)}$ nonlinearity (third-order electric susceptibility) that gives raise to the optical Kerr effect is near instantaneous, and therefore, well suited for ultrafast signal processing. It manifests as a refractive index change with optical intensity in proportion to the nonlinear index, n_2. Optical fiber also has advantages of broadband low-loss transmission and passive operation, not requiring feedback temperature control or electric biasing. On the other hand, while SOA and PPLN have typical device lengths on the order of centimeters, fiber devices based on common dispersion-shifted fiber (DSF) with nonlinearity coefficient, γ of around $3\ \mathrm{W}^{-1}\cdot\mathrm{km}^{-1}$ have required kilometer lengths to provide sufficient nonlinearity with moderate launch powers [3], [4], [12], [13], [20], [25], producing a bulky device sensitive to environmental perturbations.

Development in the late 1990s of highly nonlinear silica fibers (HNF) [26] with γ typically 3–8 times higher than DSF through combined reduction of the effective core area (A_{eff}) from $\approx$50 to $\approx$10 $\mu\mathrm{m}^2$ and enhanced n_2 by higher GeO_2 doping of the core, permitted shorter lengths of hundreds of meters [5], [6], [22]. Subsequent development of holey structured silica fibers producing high refractive index contrast between the central glass core and surrounding air holes to permit mode guidance with smaller A_{eff} increased γ even further toward $100\ \mathrm{W}^{-1}\cdot\mathrm{km}^{-1}$ [15]. Other material advances in nonsilica-based glass fibers with much higher n_2 dramatically increased γ

Manuscript received November 5, 2007; revised January 11, 2008. This work was supported in part by the Australian Research Council (ARC) under the ARC Centres of Excellence.

M. D. Pelusi, V. G. Ta'eed, E. Mägi, M. R. E. Lamont, and B. J. Eggleton are with the Centre for Ultrahigh Bandwidth Devices for Optical Systems (CUDOS), School of Physics, University of Sydney, Sydney N.S.W. 2006, Australia (e-mail: m.pelusi@physics.usyd.edu.au; vahid@physics.usyd.edu.au; magi@physics.usyd.edu.au; mlamont@physics. usyd.edu.au; egg@physics.usyd.edu.au).

L. B. Fu was with the Centre for Ultrahigh Bandwidth Devices for Optical Systems (CUDOS), School of Physics, University of Sydney, Sydney NSW 2006, Australia. He is now with IMRA America, Inc., Ann Arbor, MI 48105 USA (e-mail: ifu@imra.com).

S. Madden, D.-Y. Choi, D. A. P. Bulla, and B. Luther-Davies are with the Centre for Ultrahigh-Bandwidth Devices for Optical Systems (CUDOS), Laser Physics Centre, Australian National University, Canberra A.C.T. 0200, Australia (e-mail: sjm111@rsphy1.anu.edu.au; dyc111@rsphy1.anu.edu.au; dab124@rsphy1.anu.edu.au; bld111@rsphy1.anu.edu.au).

Color versions of one or more of the figures in this paper are available online at http://ieeexplore.ieee.org.

Digital Object Identifier 10.1109/JSTQE.2008.918669

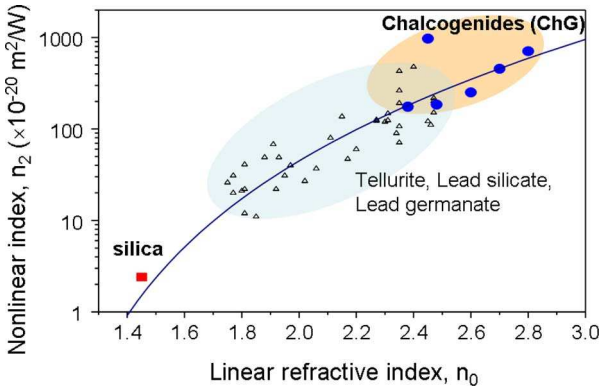

Fig. 1. (Curve) Miller's rule for nonlinearity index, n_2, versus refractive index, n_0, compared to measurements for (filled circles) various ChG glasses, (triangles) other highly nonlinear and (box) silica glasses, as in [28].

beyond another order of magnitude to $>1000\ \mathrm{W}^{-1}\cdot\mathrm{km}^{-1}$, albeit with high loss, enabling signal processing with remarkably short lengths on the order of 1 m for both Bi_2O_3 [2], [8], [9] and the chalcogenide (ChG) glass, As_2Se_3 [17] fibers. ChG glasses [27] are of particular interest for their ultrahigh n_2 measured to be up to three orders of magnitude greater than silica, in accordance with Miller's rule for such high refractive index glasses (>2.2), as plotted in Fig. 1 [28].

To even further enhance the γ of such fibers, the cross-sectional power density of the propagating mode can be raised by reducing A_{eff} through either a holey structure design [28] or tapering of the waist diameter, as was previously demonstrated for silica [29] and Bi_2O_3 fibers [30]. Application to ChG fibers is aided by its higher refractive index for enabling mode confinement in smaller diameter fibers as was shown by the extreme tapering of a 165-μm diameter As_2Se_3 fiber to nanowire size that produced dramatic increase in γ from 1200 to 68000 $\mathrm{W}^{-1}\cdot\mathrm{km}^{-1}$, albeit with limited power handling [31].

Beyond even shorter device lengths, challenge remains for shrinking optical waveguides from discrete fiber devices onto a planar platform whereupon integration of multisignal processing functions or parallel optical circuits for processing different wavelength signals simultaneously on a single photonic chip can be envisioned. This calls for more advanced waveguides exhibiting both ultrahigh nonlinearity and low loss to ensure low operating power. Recent progress in silicon rib waveguides has demonstrated fabrication of nanowire dimension photonic circuits enabling sufficient nonlinearity in centimeter lengths, albeit with quite high losses, for applications in all-optical wavelength conversion [16] and phase conjugation [21] at 10–40 Gb/s. However, silicon also suffers significant nonlinear losses from free-carrier absorption and two-photon absorption (TPA) that may impede operation at higher bit rates. In another approach, ChG rib waveguides can be fabricated to exploit the material's ultra-high n_2, and low TPA for obtaining sufficient Kerr nonlinearity in compact, ultrafast photonic circuits suited to higher bitrates [10].

In this paper, we review the development and application of highly nonlinear ChG glass devices based on both tapered fiber and planar rib waveguides in application to high-speed all-optical signal processing. Section II considers the moderate tapering of an As_2Se_3 fiber to enhance the nonlinearity and enable high-performance wavelength conversion of a 40 Gb/s signal in a shorter 16 cm device that favorably reduces the total chromatic dispersion to broaden the wavelength conversion range—the first experiment of its kind for a tapered fiber. Section III describes fabrication of As_2S_3 planar rib waveguides exhibiting nonlinearity coefficient up to $2080\ \mathrm{W}^{-1}\cdot\mathrm{km}^{-1}$, with low polarization dependence and insertion losses. The material's high refractive index, ensuring robust mode confinement, is exploited in designing a longer 22.5 cm waveguide compacted into a 7 cm chip by an advanced serpentine-shaped circuit incorporating 180° bends, while achieving a record-low loss of 0.05 dB/cm [33]. High nonlinearity for the planar waveguide is obtained with a comparatively large A_{eff} of $5-7\ \mu\mathrm{m}^2$, thereby easing demands on fabrication and coupling compared to nanowires. This leaves scope for further enhancing the nonlinearity by fabricating to smaller dimensions, which can also control the waveguiding dispersion to offset the large normal dispersion of ChG glasses to zero or anomalous values [34]. Section III also explores application of waveguides to broadband wavelength conversion of 40–80 Gb/s signals by cross-phase modulation (XPM), and optical time-division demultiplexing of a 160 Gb/s signal by four-wave mixing (FWM), and considers the optimum design for maximizing efficiency.

TABLE I
OPTICAL FIBER PARAMETERS AT 1550 NM

Parameter	Units	SiO_2 DSF	SiO_2 HNF	Bi_2O_3 fiber	As_2Se_3 fiber	As_2Se_3 taper
Nonlinear index (n_2)	n_2 of silica[a]	1	2.3	50	500	500
Effective core area (A_{eff})	$\mu\mathrm{m}^2$	60	12	4	37	20
Nonlinearity coefficient (γ)	/W/km	1.9	17.5	1360	1200	2270
Dispersion (D)	ps/nm/km	-0.7	-0.1	-260	-560	-560

[a] n_2 of silica = $2.2\times10^{-20}\mathrm{m}^2/\mathrm{W}$ at 1550 nm.

II. Tapered As_2Se_3 Fiber Waveguides

A. Fabrication

Enhanced γ through smaller A_{eff} by tapering is applied to a commercially available multimoded ChG glass fiber fabricated with a core and cladding of slightly different As_2Se_3 stoichiometry (nominal refractive index of 2.8) and specified diameters 7.5 μm and 165 μm, respectively. Its corresponding numerical aperture (NA) is $\approx$0.2, and measured propagation losses and fiber dispersion are $\approx$1 dB/m and $D=-560\ \mathrm{ps}\cdot\mathrm{nm}^{-1}\cdot\mathrm{km}^{-1}$ respectively, at 1550 nm wavelength.

Table I compares the parameters for various highly nonlinear fiber compositions, highlighting the orders of magnitude greater than n_2 for As_2Se_3 compared to the widely reported Bi_2O_3. It is noted that the nonlinearity coefficient defined as $\gamma=(2\pi/\gamma)\cdot(n_2/A_{\mathrm{eff}})$ [35] at optical wavelength, λ, is smaller

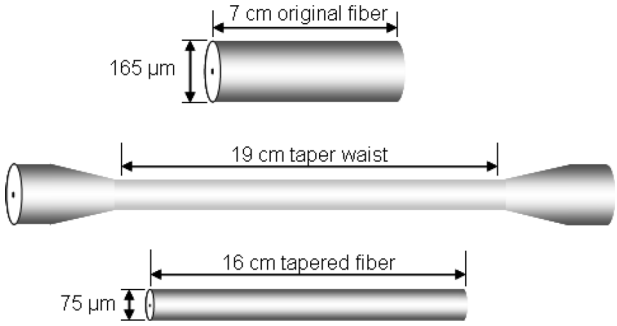

Fig. 2. Steps for tapering an As_2Se_3 fiber to narrower diameter.

for As_2Se_3 than Bi_2O_3, due to its much larger A_{eff} of 37 μm^2. Nevertheless, its higher linear refractive index gives wider scope for dramatically increasing γ through reduced A_{eff} without compromising mode confinement. This contrasts with the already much smaller core sizes utilized for silica and Bi_2O_3. The nonlinear figure of merit (FOM $= n_2/\lambda\beta$) proportional to n_2 and TPA coefficient (β), is also relatively low for As_2Se_3 compared to Silica and Bi_2O_3.

The low transition temperature for ChG glasses of ≈200 °C favorably permits fiber tapering by resistive heating rather than the hotter gas flame required for silica [29]. A piece of As_2Se_3 fiber was fixed between two translation stages mounted on the same rail and sandwiched in close proximity between the heaters that were programmed to raise the fiber temperature in tandem with the back and forth sliding motion of the stages in an orchestrated heat brushing routine that stretched the fiber to the desired taper profile. The maximum length of the tapered waist region obtained was constrained by the rail length.

Fig. 2 shows the schematic steps used to fabricate a 16 cm taper. The 165-μm cladding diameter of a 7-cm long fiber was tapered down to a uniform waist of 75 μm over 19 cm without incurring any noticeable increase in loss. A 16 cm portion was cleaved and respliced onto single-mode silica fiber, using UV-cured epoxy to achieve a stable low insertion loss of ≈5 dB (2.5 dB best to date for similar tapers). Mode field imaging indicated single-mode operation, and comparison with known fiber (Corning SMF-28) indicated a mode field diameter of 5-μm corresponding to $A_{\text{eff}} \approx 20\,\mu\text{m}^2$ yielding an increase in nonlinearity coefficient from 1200 to $\approx 2270\,\text{W}^{-1}\cdot\text{km}^{-1}$.

Mode analysis by the finite-element method for A_{eff} as a function of tapered fiber diameter and numerical aperture (NA) predicted similar results and showed further decreasing A_{eff} would require more extreme tapering to waist diameters narrower than several micrometers [31], at which point guiding is by the cladding–air interface rather than the core. Simultaneously, the role of waveguiding dispersion, while negligible for the 16 cm taper, grows dramatically for sub-10-μm waist diameters and counter to the material normal dispersion enabling tailoring of the device dispersion to zero or anomalous value [31].

B. 40-Gb/s Wavelength Conversion in Tapered Fiber

Applying the 16-cm length taper to all-optical wavelength conversion of a 40-Gb/s return-to-zero (RZ) format signal

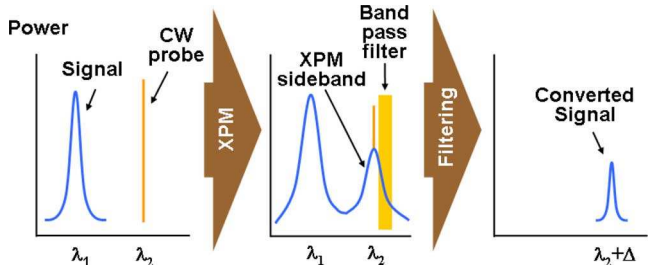

Fig. 3. Principle of wavelength conversion by XPM and optical filtering.

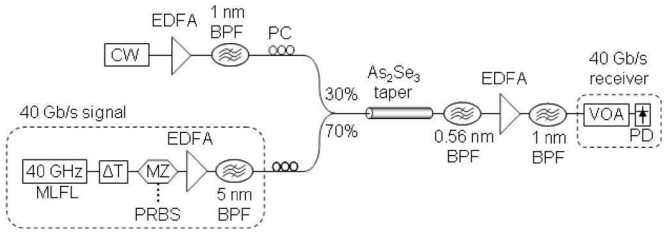

Fig. 4. Experimental setup for 40-Gb/s wavelength conversion in a 16-cm length tapered As_2Se_3 fiber.

was performed by the technique originally demonstrated for a 40 Gb/s signal with a 10 km DSF [13]. The principle is schematically shown in Fig. 3, whereby the signal is copropagated through the nonlinear waveguide with a continuous-wave (CW) laser tuned to the desired output wavelength. By the Kerr effect [35], XPM from each signal pulse induces a transient chirp at the coincident point along the CW beam generating frequency-modulated sidebands that can be converted to amplitude modulation by optical filtering to recover a replica of the signal at different wavelengths.

The experimental setup using the fiber taper is shown in Fig. 4. The RZ signal was generated from a 40-GHz actively mode-locked fiber laser (MLFL) emitting 1.5-ps duration pulses of 1.6 nm bandwidth centered at 1535 nm. An external electrooptic Mach–Zehnder (MZ) modulator driven by a 40-Gb/s pattern generator encoded a pseudorandom bit sequence (PRBS) of length $2^{31}-1$ on the pulses. The signal was amplified by an Erbium-doped fiber amplifier (EDFA) and passed through a 5-nm tunable bandpass filter (BPF) to remove out of band-amplified spontaneous emission noise before being combined with the amplified, wavelength-tunable, CW laser. The average launch power to the taper was 130 mW for the signal (≈73 mW in the taper, 2.3W peak) and 50 mW for the CW laser (≈28 mW in the taper). The converted signal was obtained using a 0.56 nm bandwidth, tunable BPF to extract a sideband from the spectrally broadened CW probe, which was then amplified and passed through a second 1-nm bandwidth-tunable BPF, connected before a variable optical attenuator (VOA) and 40 Gb/s photodetector (PD).

Fig. 5 compares the output spectra from the As_2Se_3 taper for different CW laser wavelengths up to 35 nm from the signal. A noticeable reduction in spectral broadening of the CW beam was observed at wavelengths longer than 1560 nm due to the effect of chromatic dispersion causing the coincidence of the signal pulses with the CW to shift during propagation in the

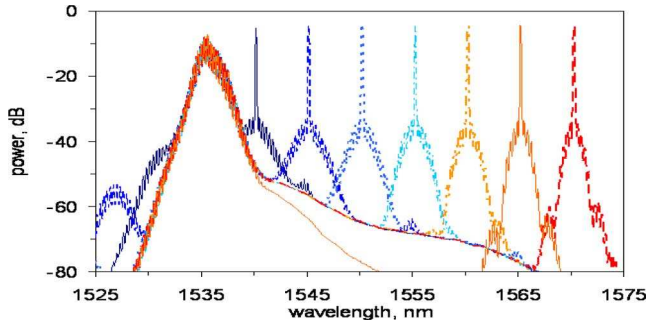

Fig. 5. Overlaid output optical spectra from a 16-cm length As_2Se_3 fiber taper for different CW wavelengths with 40 Gb/s signal fixed at 1535 nm.

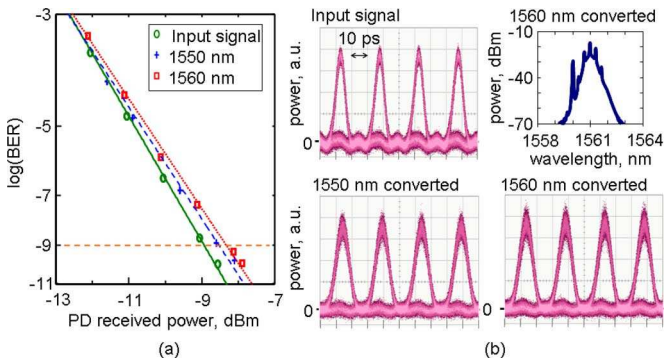

Fig. 6. (a) BER performance of wavelength-converted 40 Gb/s signals from 16 cm As_2Se_3 fiber taper and (b) 40-Gb/s signal eye diagrams at converted and original wavelengths, and converted spectrum.

waveguide, smearing the XPM chirp. The reduced interaction length can be estimated using $L_w = T_{\mathrm{FWHM}}/\Delta\lambda \cdot D$ where T_{FWHM} is the full-width at half-maximum of the pulse, $\Delta\lambda$ its wavelength offset to the CW, and D the waveguide dispersion (differential of group delay with wavelength), which is assumed to vary negligibly across $\Delta\lambda$. For the experimental parameters, L_w becomes favorably longer than the waveguide for $\Delta\lambda < 17$ nm. This contrasts with the previously reported 10-Gb/s wavelength conversion of 7 ps pulses using 1 m of untapered As_2Se_3 fiber [17] that demonstrated a narrower wavelength tuning range despite the more than quadruple T_{FWHM} explained by the calculated $\Delta\lambda$ <12.5 nm for $L_w > 1$ m.

The eye diagrams of the converted 40 Gb/s signals obtained in Fig. 6 show only slight degradation compared to the original 40 Gb/s signal, and the bit-error rate (BER) performance shows a small power penalty of just 0.4 dB at a BER of 10^{-9} compared to connecting the 40 Gb/s signal directly from the MZ modulator to the receiver. This marks a significant improvement over the 1.4 dB penalty measured for the 10 Gb/s conversion in untapered fiber [17], thanks to the broader XPM spectral broadening associated with the shorter signal pulses.

Increasing the signal bit-rate to 160 Gb/s with the same pulse source would increase the duty cycle (pulse duration to period ratio) from 6% to 24%. Although L_w would be unchanged, maintaining equivalent XPM sideband power at the waveguide output, and therefore, the same optical SNR (OSNR) at the receiver would require quadrupling the launch power to ~500 mW, which exceeds its maximum safe power handling limit. Tapering the fiber to nanowire dimensions could enhance γ by more than an order of magnitude, and reduce launch powers by the same factor, but unfortunately, reduce the power handling as well.

TABLE II
CHALCOGENIDE WAVEGUIDE COMPARISON

Parameter	Units	As_2Se_3 taper	As_2S_3 rib (2.7×3.8 μm)	As_2S_3 rib (2.6×4 μm)
Length (L)	cm	16	5	22.5
Insertion Loss	dB	5	7.5	6.5
Refractive Index (n)	-	2.8	2.37	2.37
Nonlinear index (n_2)[a]	n_2 of silica	500	132	132
Effective core area (A_{eff})	μm^2	20	5.7	7.1
Nonlinearity coefficient (γ)[†]	W^{-1} km^{-1}	2270	2080	1700
Dispersion (D)[†]	ps/nm/km	-560	-286	-342

[a] n_2 of silica = 2.2×10^{-20} m^2/W at 1550 nm wavelength
[†] at 1550 nm wavelength

III. PLANAR As_2S_3 RIB WAVEGUIDES

A. Fabrication

In another approach, planar rib ChG waveguides were fabricated by photolithographic mask patterning and etching of ChG thin films deposited on oxidized silicon wafer. Two customized methods; ultrafast pulsed laser deposition (UPLD) [32] and thermal evaporation deposition [33] were explored to create films of thickness up to several micrometers that were then annealed to raise the refractive index closer to bulk As_2S_3 glass. Standard photolithography followed by dry etching using inductively coupled plasma reactive ion etching technique produced a series of high-quality rib waveguides of various widths and lengths on each wafer. The waveguides were overclad with a 15-μm thick film of UV-cured inorganic polymer glass, whose refractive index is 1.53 compared to 2.37 for the As_2S_3 film at 1550 nm. End facets were then finished by hand cleaving the silicon substrate with a diamond scriber.

Table II lists the parameters of two As_2S_3 waveguides obtained, along with the tapered ChG fiber, described in Section II for comparison. The first denoted W5 was a 5-cm length rib formed in a UPLD film of 2.7 μm thickness by etching out 1.2-μm deep trenches on either side of a 3.8-μm wide rib. The second denoted W22 was a longer 22.5 cm rib formed in a thermally deposited film of 2.6 μm thickness, by etching out 0.9-μm deep trenches on either side of a 4-μm wide, serpentine-shaped rib. Fig. 7 shows a micrograph of the W22 waveguide-cleaved cross section, and Fig. 7(b) shows the waveguide schematic incorporating three straights sections linked by two 180° bends of radii ≈3 mm for accommodating a 7-cm size chip.

The A_{eff} of the transverse electric (TE) mode for both W5 and W22 waveguides were calculated based on physical dimensions using c2V Olympios software to be 5.7 μm^2 and 7.1 μm^2 respectively at 1550 nm. The nonlinear refractive index of As_2S_3 given by $n_2 = 2.92 \times 10^{-18}$ m^2/W [32], is more than two

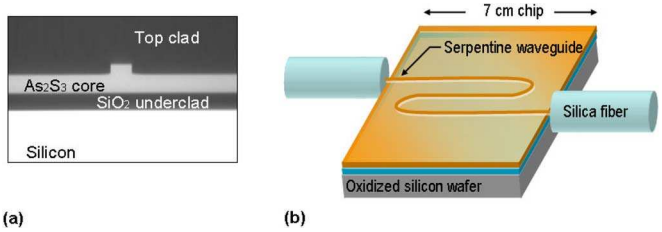

Fig. 7. ChG planar rib waveguide (W22) obtained from thermally deposited As_2S_3 film. (a) Optical micrograph of cleaved facet. (b) Circuit schematic.

orders of magnitude greater than silica, yielding corresponding nonlinear coefficients of 2080 and 1700 $W^{-1} \cdot km^{-1}$ respectively.

The material dispersion, determined from refractive index measurements of the deposited As_2S_3 films and polynomial curve fitting to its wavelength differential, was found to be $\beta_2 = 469\,ps^2/km$ corresponding to a normal dispersion of $D = -368$ ps/nm.km. Numerical analysis by the finite-element method of the mode profiles generated for the physical waveguide dimensions, suggest significant waveguiding dispersion of opposite sign to the normal material dispersion that reduces total β_2 to 364 ps^2/km^2 and 433 ps^2/km for W5 and W22 waveguides, respectively—similar to Bi_2O_3 fiber [2], [8], [9].

The TE mode propagation losses were measured by the Fabry–Perot resonance technique [36] to be 0.25 and 0.05 dB/cm, respectively, at 1550 nm for W5 and W22 waveguides, with polarization-dependent losses (PDL) between TE and TM modes of 1 dB and 2.4 dB, respectively. The five times lower loss for the W22 waveguide is the record lowest reported for As_2S_3 to date and was realized through combined improvements in deposition of higher quality films as well as photolithography and optimization of the reactive ion etching chemistry, which reduced the rib sidewall roughness to just 1.5 nm (rms) [33]—more than a factor of two improvement over the W5 waveguide [32].

Low loss coupling to standard single-mode fiber (Corning SMF-28) was achieved via an intermediate fusion-spliced section of higher NA fiber (NA = 0.35) butt coupled to the waveguide for improved mode matching and use of index matching oil to reduce reflections. Fiber-to-fiber insertion losses were ≈7.5 dB and 6.5 dB for W5 and W22 waveguides, respectively, with ≈1.1 dB constituting propagation loss.

B. 40–80-Gb/s Wavelength Conversion in Rib Waveguides

The record low loss of the W22 waveguide enables the nonlinear effect to be sustained along its entire 22.5 cm length thereby maximizing the nonlinear phase shift for a given launch power. Its effectiveness was demonstrated in all-optical wavelength conversion of 40 Gb/s signals in a similar manner to the tapered fiber experiment described in Section II with a setup similar to Fig. 4 [19]. To consider a more realistic signal duty cycle, the 5 nm BPF in the transmitter was substituted with two 1-nm bandwidth BPFs (both of 1st-order Gaussian profile and tuned to the signal center wavelength), in order to narrow the 40-Gb/s signal spectrum and broaden the pulse duration to 4.4 ps,

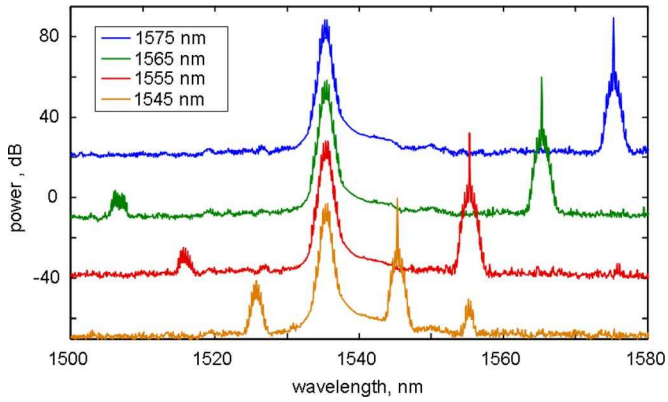

Fig. 8. Output optical spectra from 22.5-cm length As_2S_3 rib waveguide at different CW wavelengths with 40 Gb/s signal fixed at 1535 nm.

for a higher duty cycle of 18%. Doing so favorably nullified the walkoff effect and broadened the wavelength tuning range as expected from the calculated $\Delta\lambda < 58$ nm for $L_w > 22.5$ cm. However, maintaining equivalent XPM spectral broadening required a commensurate increase in average launch power by the pulse broadening factor. Best results were obtained with EDFAs operating near saturation to give average launch to the waveguide facet of 240 mW for the signal (≈129 mW average, 1.4 W peak coupled in) and 90 mW for the CW laser. The combined total of 330 mW is significantly higher than the 180 mW for the tapered fiber experiment, which was a conservative limit set to avoid gradual increased insertion loss possibly due to photodarkening of the material [27].

Fig. 8 plots the output spectra from the W22 waveguide for the signal at 1535 nm wavelength and the CW laser tuned between 1545 and 1575 nm. It shows similar XPM spectral broadening of the CW laser at wavelengths out to 1575 nm—limited by both the gain bandwidth of the EDFAs (which accounts for increasing noise) and tuning range of the thin-film type BPFs.

The frequency-modulated sideband of the CW containing the converted signal was extracted using the two BPFs of optical bandwidth 0.56 and 1 nm, as shown in Fig. 4. The converted signal eye diagrams shown in Fig. 9 indicate only slight degradation compared to the tapered fiber results in Fig. 6. The BER curves plotted in Fig. 9 indicate a power penalty of ≈1 dB at a BER of 10^{-9} when compared to connecting the 40 Gb/s signal directly to the VOA and PD.

The capability for applying the W22 waveguide to higher bit-rate wavelength conversion at 80 Gb/s was investigated using the slightly modified setup in Fig. 10 with the signal at 1550 nm. A fiber-delay interferometer of 2^7-1 bit delay was inserted after the MZ modulator to optically multiplex (MUX) the 40 Gb/s signal to 80 Gb/s. Inserting a broader 8 nm BPF in the transmitter ensured a shorter signal pulse duration of 1.5 ps, thereby maintaining a comparable duty cycle of 16% as the 40 Gb/s experiment. This, therefore, ensured a similar peak to average power ratio, with tradeoff narrowing of the wavelength-conversion range as expected from the calculated $\Delta\lambda < 20$ nm for $L_w > 22.5$ cm. The average power launched to the waveguide facet was slightly increased from the 40 Gb/s experiment to 270 mW for the 80 Gb/s signal (≈2.3 W peak coupled in),

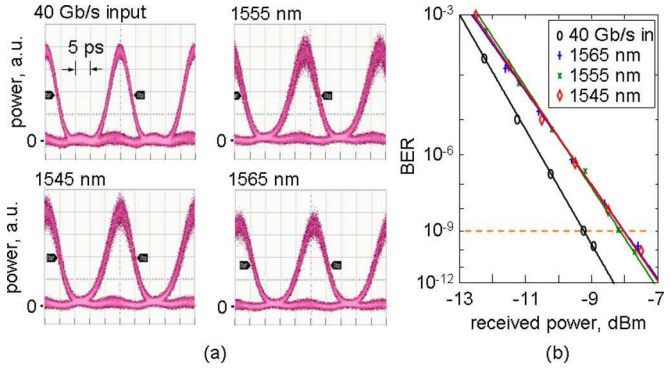

Fig. 9. (a) 40-Gb/s signal eye diagrams at converted and original wavelengths from 22.5-cm length As_2S_3 rib waveguide. (b) BER performance of wavelength-converted 40 Gb/s signals.

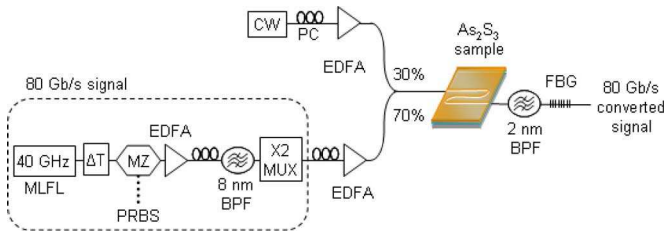

Fig. 10. Experimental setup for 80-Gb/s wavelength conversion in 22.5-cm length As_2S_3 waveguide.

and 150 mW for the CW for combined total of 420 mW. The 80 Gb/s wavelength-converted spectra at the waveguide output were filtered using a 2 nm BPF followed by a fiber Bragg grating (FBG) notch filter to reject the CW. Fig. 11(a) compares the output spectra for different CW wavelengths and shows consistent XPM broadening across the full-gain bandwidth of the EDFA up to 1570 nm. The converted signal eye diagrams in Fig. 11(b) show noticeably higher noise than for the 40 Gb/s experiment, due to the lower sideband power obtained from the broader BPFs used and corresponding larger noise introduced by the EDFAs.

Wavelength converting a 160-Gb/s RZ signal of the same pulse duration using the same waveguide would require doubling the signal power, which would exceed the saturation power of the EDFAs and maximum safe handling power to avoid damaging the waveguide facet; as well as potentially increasing the insertion loss due to photodarkening of the As_2S_3 thin films, which has been reported as having a threshold peak power of $\approx 10\ \mathrm{W}/\mu\mathrm{m}^2$ [37].

Similar wavelength conversion performance has been demonstrated using the shorter W5 waveguide, but at a lower signal bit rate of 10 Gb/s and with shorter 2 ps pulses in order to increase the peak to average power ratio and ensure sufficient XPM sideband power for a lower total average launch power of ≈140 mW [18]. While the shorter device length favorably negated the impact of the shorter pulses on the wavelength conversion range, the overall nonlinearity was insufficient for extending the bit rate to 40 Gb/s and beyond for the same average launch power.

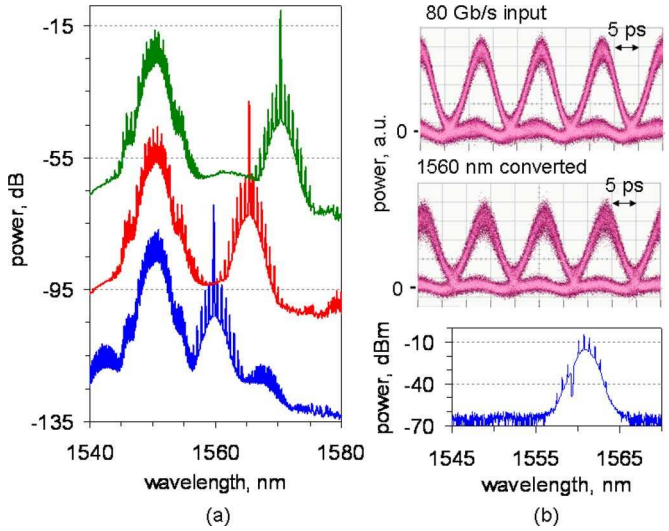

Fig. 11. 80-Gb/s wavelength conversion in 22.5-cm length As_2S_3 waveguide. (a) Output optical spectra at different CW wavelengths for signal fixed at 1535 nm. (b) 80-Gb/s signal eye diagrams with converted signal spectra.

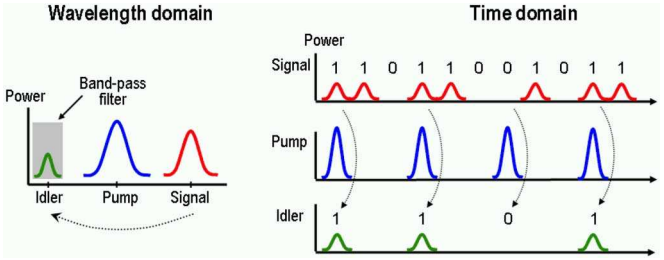

Fig. 12. Principle of all-optical time-division demultiplexing of an optical signal by FWM with binary data levels indicated by "1"and "0".

C. 160 Gb/s Demultiplexing in Rib Waveguides

The optical Kerr effect that produced XPM in the W22 waveguide enabling 40–80 Gb/s wavelength conversion in Section III–B, also gave rise to four-wave mixing (FWM) wavelength conversion [12], evident from the output spectra in Fig. 8 showing generation of a replica signal at shorter wavelengths than the original. However, the effect was dwarfed by XPM, and diminished sharply for wider tuning offset of the CW laser due to the dispersion of the waveguide. For the same reason, it is also highly sensitive to the waveguide length on the centimeter scale. The following experiment shows such effect can be utilized in the shorter W5 waveguide to enable optical time-division demultiplexing of a 160-Gb/s optical signal to its 10-Gb/s tributaries.

All-optical demultiplexing by FWM was originally demonstrated in fiber [3] applying the principle illustrated in Fig. 12, whereby a high-bit rate signal with carrier frequency f_s is co-propagated with a pump pulse train of subharmonic repetition rate and carrier frequency, f_p. By delaying the pump pulses to coincide with the desired subharmonic bit-rate channel of the signal to be extracted, FWM between coinciding signal and pump pulse generates a new idler pulse with carrier frequency f_i given by $f_i = 2f_p - f_s$ [35]. This thereby generates a signal

channel that can be filtered out and switched to a receiver or rerouted without requiring electronic detection and regeneration of the entire optical signal. High performance requires minimizing intrachannel interference by using pump pulses of narrower duration than the signal bit period and of suitably low jitter to ensure coincidence with only a single signal pulse during propagation through the waveguide. Earlier experiments used kilometers of DSF [3], while a more recent 160 Gb/s demonstration required just 1 m of Bi_2O_3 fiber [9]. Minimizing the device length for broadband applications is essential for maximizing FWM when the device has such a large dispersion parameter.

The maximum energy transfer from the original signal to the idler by FWM relies upon adequate phase matching between all-optical waves (signal, pump, and idler). This can be expressed by the wave vector mismatch in terms of the propagation constants for the pump (β_p), signal (β_s) and idler (β_i) as $\Delta\beta = \beta_s + \beta_i - 2\beta_p$ [35]. The propagation length, L, satisfying phase-matched FWM is then determined by the coherence length, $L_{\rm coh}$ defined as [35]

$$L \le L_{\rm coh} = \frac{2\pi}{|\Delta\beta|}. \tag{1}$$

When $\Delta\beta$ is dominated by the dispersion of the medium, which, in turn, is dominated by the second-order dispersion coefficient (β_2) of the Taylor series expanded mode propagation constant [35] with higher order terms negligible, $L_{\rm coh}$ can be expressed approximately in terms of the angular frequency separation, Ω_S, corresponding to $f_{\rm p} - f_{\rm s} = f_{\rm i} - f_{\rm p}$ as

$$L_{\rm coh} \approx \frac{2\pi}{|\beta_2|\,\Omega_s^2} \tag{2}$$

Considering FWM-demultiplexing of a 160-Gb/s RZ format optical signal, spectral overlap between pump and signal is comfortably avoided for $f_p - f_s$ corresponding to 10 nm wavelength separation giving $L_{\rm coh}$ of 28 and 24 cm for W5 and W22 waveguides respectively, which suggests W22 is less optimal.

Further insight is gained by calculating the theoretical conversion efficiency, G_c, as a function of L assuming undepleted pump (i.e., power of pump $\gg$ signal) of peak power, P_p, zero propagation loss, and same overlapping integrals for the cross-sectional mode profiles of all waves, whereby the equation is given by [35]

$$G_C = (\gamma \times P_P/g)^2 \times \sin^2(g \times L) \tag{3}$$

where g is the parametric gain coefficient defined as [35]

$$g^2 = \Delta\beta\,(\Delta\beta/4 + \gamma P_P)\,. \tag{4}$$

Fig. 13(a) plots G_c versus distance for parameters of both the W5 and W22 waveguides listed in Table II for $P_p = 4.4\,\mathrm{W}$ as applied in the later 160 Gb/s experiment. The curves show slightly higher FWM efficiency for W5 at 5 cm distance than for W22 at 22.5 cm. The impact of propagation losses with coefficient, α, on the conversion efficiency can be inferred from the modified equations given by [38]

$$G'_C = (\gamma \times P_P/g')^2 \times \exp(-3\alpha L) \times \sin^2(g' \times L) \tag{5}$$

where

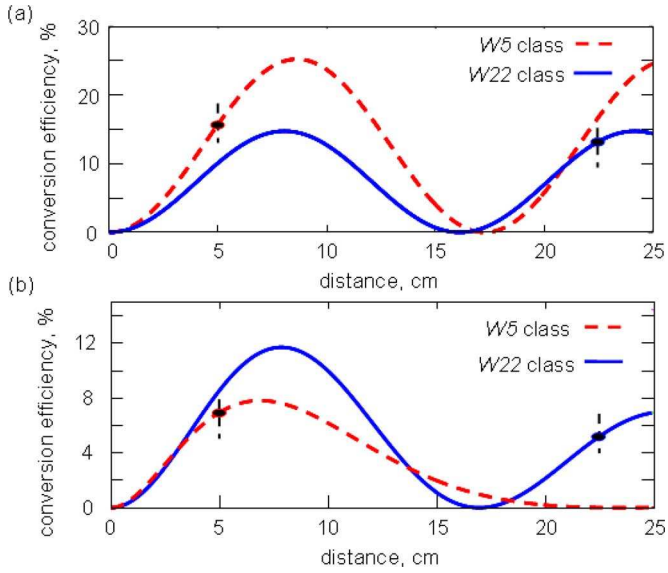

Fig. 13. Conversion efficiency versus propagation distance in case of $f_{\rm p} - f_{\rm s} \Leftrightarrow 10$ nm calculated for parameters of both the W5- and W22-type waveguides with propagation losses set to (a) zero and (b) Table II values.

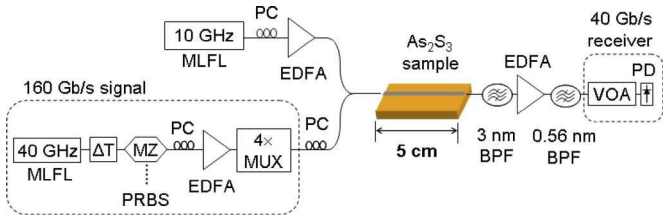

Fig. 14. Experimental setup for 160-Gb/s optical time-division demultiplexing by FWM in 5-cm length As_2S_3 waveguide.

$$(g')^2 = \Delta\beta\,(\Delta\beta/4 + \gamma P_P \times \exp(-\alpha L))\,. \tag{6}$$

Fig. 13(b) shows conversion efficiency is just slightly higher for W5 at 5 cm than W22 at 22.5 cm, but 33% less than what could be obtained with W22 at 8 cm length.

The setup for 160 Gb/s FWM-demultiplexing using the W5 waveguide is shown in Fig. 14. The 160 Gb/s signal was generated from the 40 GHz MLFL emitting 1.4 ps pulses with 1.8 nm bandwidth centered at 1560 nm wavelength. The MZ modulator encoded data on the pulses at 40 Gb/s with a $2^{31}-1$ PRBS, and the two-stage MUX of 2^7-1 bit delay length interleaved the signal up to 160 Gb/s bit rate. The pulse width at waveguide input was 1.9 ps corresponding to a 30% duty cycle.

The pump source was a 10-GHz MLFL emitting pulses of 1.5 nm bandwidth centered at 1550 nm wavelength and was synchronized to the 160 Gb/s signal by operating from the same 40 GHz RF clock, prescaled to 10 GHz (in place of using a 10-GHz clock recovery circuit). Signal and pump were amplified with EDFAs, then combined with a coupler, and launched into the waveguide with polarization states aligned via polarization controllers (PC). The pump pulses at coupler output were 1.5 ps wide with average power set to 150 mW, giving $P_p \sim 4.4$ W in the waveguide. An optical delay line (ΔT) aligned the pump pulses with the desired channel of the 160 Gb/s signal

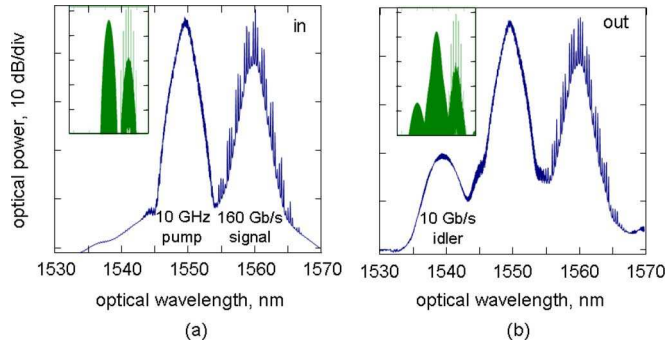

Fig. 15. Optical spectra at (a) Input. (b) Output of 5-cm length As_2S_3 waveguide with (inset) numerically simulated equivalent for W5 waveguide and 160 Gb/s signal parameters (40-nm wavelength span, 10 dB/div power).

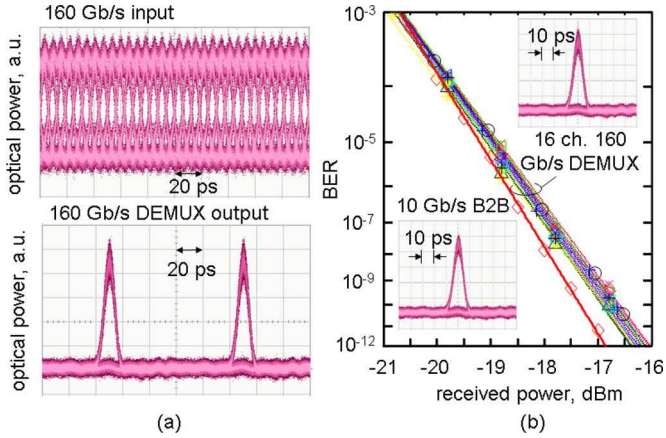

Fig. 16. (a) Eye diagrams of (top) input 160-Gb/s signal (lower) demultiplexing output 10 Gb/s channel. (b) 160 Gb/s demultiplexing BER performance compared to back-to-back (B2B), (inset) 10-Gb/s eye diagrams.

to be demultiplexed. Signal power was set to 100 mW average (≈0.3 W peak coupled in) for a combined total of 250 mW.

The optical spectra at input and output of the waveguide are compared in Fig. 15, and indicate negligible self-phase modulation (SPM) [35] and XPM for the optimized launch powers, while significant idler power was generated at 1540 nm. In contrast, time-division demultiplexing by XPM either with optical filtering as reported for a 80 Gb/s signal using a 5 km DSF [4] or in a nonlinear optical fiber loop mirror [4] would require significantly higher launch power, and corresponding wider wavelength separation between the signal and pump to accommodate their spectral broadening without overlap.

The power conversion efficiency of the 10 Gb/s channel from 1560 nm to 1540 nm wavelength was calculated to be 12% by integrating powers of both the measured optical spectra of the input 160 Gb/s signal and output idler and accounting for the 16 times difference in bit rate. This compares well to the generalized theoretical lossless and lossy values of $G_c = 15.8\%$ and $G_c' = 7\%$, respectively. Numerical modeling of 160 Gb/s FWM-demultiplexing by the split-step Fourier method [35] using the same experimental parameters for both waveguide and signal (assuming Gaussian pulse shape) without noise or polarization effects also generated qualitatively similar spectra as shown in Fig. 15, with G_c equal to 11% and 7% for propagation loss set to 0 dB/cm and 0.25 dB/cm, respectively. Similarly, numerical calculations of G_c versus L for 160 Gb/s demultiplexing give reasonable fit to the Fig. 13 curves.

The quality of the FWM idler extracted from the output spectra using two optical band pass filters (BPF) of bandwidth 3 nm and 0.56 nm, is highlighted by the signal eye diagrams in Fig. 16(a) of both the 160 Gb/s input and the 10 Gb/s output measured using a 65 GHz bandwidth PD on an 80-GHz electrical sampling scope. The 10-Gb/s eye diagram shows a clear opening with just slightly more noise compared to the "back-to-back" (B2B) obtained for the 10 GHz MLFL tuned to 1540 nm wavelength, data modulated at 10 Gb/s, and passed through the same BPFs. Fig. 16(b) reveals a small power penalty of <1 dB at BER of 10^{-9} for all 16 channels of the 160 Gb/s signal thanks largely to the near-instantaneous Kerr nonlinearity ensuring low crosstalk. Connecting the MZ modulator output directly to PD improves B2B receiver sensitivity by just 0.4 dB compared to the curve plotted in Fig. 16(b). This result marks the shortest length demonstration of nonlinear-Kerr-effect-based signal processing at such a high-signal bit rate reported to date.

A route to reduce pump power requirements or achieve higher FWM conversion efficiency over a wider bandwidth is by tailoring the waveguide design to narrower dimensions for both increasing the nonlinearity through its reduced A_{eff}, and exploiting the waveguide dispersion that grows dramatically as dimensions approach the optical wavelength, and counter to the material dispersion. Simulation analysis suggests As_2S_3 rib waveguides designed for moderately smaller A_{eff} of 1–2 μm^2 could achieve zero or even anomalous dispersion, to enable broadband parametric gain [34]. It would also broaden the tuning range for both XPM- or FWM-based signal processing applications and higher bit-rate operation. Longer circuits could also be applied to further increase the net nonlinearity or reduce launch powers.

IV. Discussion

The experiments described in Sections II and III showed the best choice of waveguide for XPM- or FWM-based signal processing depends on the signal bit rate and dispersion in addition to the maximum nonlinear Kerr effect obtained. Reducing the waveguide dimensions and corresponding A_{eff} through fiber tapering or finer photolithographic etching provides a route to enhance the nonlinearity coefficient, and simultaneously tailor the dispersion to zero or anomalous value when dimensions approach the order of the optical wavelength. Such combined advances would further lower the operating power and enable more broadband operation.

Further reducing A_{eff} for the tapered As_2Se_3 fiber would require a leapfrog reduction of the fiber diameter from 75 μm down to several micrometers or less [31]. ChG nanowires exhibiting nonlinearity coefficients of 68 000 $\text{W}^{-1} \cdot \text{km}^{-1}$ could, in principle, reduce the average powers for the same experiments with same length waveguides studied in this paper by more than an order of magnitude to around 10 mW, but would require advances

in raising the average power handling to avoid thermal damage by inadequate heat dissipation into the surrounding air.

Shrinking the dimensions of planar waveguides may not be as susceptible to such heat dissipation issues due to the large thermal mass of the substrate. Reducing A_{eff} from current $5-7\ \mu\text{m}^2$ is a path to higher nonlinearity coefficient, at the expense of increasing propagation losses as dimensions become more appreciable to the side-wall roughness. However, analysis of the current waveguide dimensions shows that, unlike for nanowires, only the tails of the cross-sectional mode distribution permeate to the side walls, which suggests some margin for reducing waveguide dimensions with only slight increase in losses [33]. Nevertheless, smaller A_{eff} would require a more sophisticated coupling system to minimize losses that could otherwise trump any nonlinearity gain.

As Table II shows, the As_2Se_3 fiber taper had the highest nonlinearity coefficient of all three waveguides considered, as well as lowest fiber-to-fiber insertion loss ($<$5 dB), but average power handling was conservatively about half that of the planar waveguides. The 18% lower nonlinearity coefficient for the 22.5-cm length As_2S_3 waveguide compared to the 5 cm device, was offset by the more than quadruple length and record low 0.05-dB/cm propagation loss. On the other hand, its higher net chromatic dispersion impacted FWM efficiency, which was higher for the 5-cm length device.

A narrower waveguide that gains factor of two higher nonlinearity or lower dispersion could permit increase of the signal bit rate in the various applications including time-division demultiplexing, XPM-based wavelength conversion, or SPM based all-optical regeneration [1], [2]. ChG-based waveguides can exploit the higher refractive index to allow more complex, and longer yet compact nonlinear circuits, and also utilize the reported high photosensitivity of the material [37] for incorporating on-chip Bragg grating optical filters [1].

V. Conclusion

Highly nonlinear ChG waveguides based on both planar rib and tapered optical fiber waveguides of 5–22 cm length have been produced exhibiting nonlinearity coefficients of 1700–2270 $\text{W}^{-1} \cdot \text{km}^{-1}$. Application to nonlinear signal processing exploiting both XPM and FWM enabled broadband wavelength conversion of 40–80 Gb/s signals and high-performance time-division demultiplexing of a 160 Gb/s signal. Future potential exists for tailoring the dimensions of these waveguides to further increase the nonlinearity and simultaneously reduce the normal dispersion parameter. This will enable operation at higher bit rates with lower launch powers as well as broaden the wavelength tuning range and extend potential application to other nonlinear signal processing functions such as all-optical SPM-based regeneration and FWM-based optical phase conjugation.

References

[1] V. G. Ta'eed, M. Shokooh-Saremi, L. Fu, I. C. M. Littler, D. J. Moss, M. Rochette, B. J. Eggleton, Y. Ruan, and B. Luther-Davies, "Self-phase modulation-based integrated optical regeneration in chalcogenide waveguides," *IEEE J. Sel. Topics Quantum Electron.*, vol. 12, no. 3, pp. 360–370, May–Jun. 2006.

[2] F. Parmigiani, S. Asimakis, N. Sugimoto, F. Koizumi, P. Petropoulos, and D. J. Richardson, "2R regenerator based on a 2-m-long highly nonlinear bismuth oxide fiber," *Opt. Express*, vol. 14, pp. 5038–5044, 2006.

[3] S. Kawanishi, H. Takara, T. Morioka, O. Kamatani, and M. Saruwatari, "200 Gbit/s, 100 km time-division-multiplexed optical transmission using supercontinuum pulses with prescaled PLL timing extraction and all-optical demultiplexing," *Electron. Lett.*, vol. 31, pp. 816–817, 1995.

[4] B. E. Olsson and D. J. Blumenthal, "All-optical demultiplexing using fiber cross-phase modulation (XPM) and optical filtering," *IEEE Photon. Technol. Lett.*, vol. 13, no. 8, pp. 875–877, Aug. 2001.

[5] H. Sotobayashi, C. Sawaguchi, Y. Koyamada, and W. Chujo, "Ultrafast walk-off-free nonlinear optical loop mirror by a simplified configuration for 320-Gbit/s time-division multiplexing signal demultiplexing," *Opt. Lett.*, vol. 27, pp. 1555–1557, 2002.

[6] J. Li, B. E. Olsson, M. Karlsson, and P. A. Andrekson, "OTDM demultiplexer based on XPM-induced wavelength shifting in highly nonlinear fiber," *IEEE Photon. Technol. Lett.*, vol. 15, no. 12, pp. 1770–1772, Dec. 2003.

[7] Y. Fukuchi, T. Sakamoto, K. Taira, and K. Kikuchi, "All-optical time-division demultiplexing of 160 Gbit/s signal using cascaded second-order nonlinear effect in quasi-phase matched $LiNbO_3$ waveguide device," *Electron. Lett.*, vol. 39, pp. 789–790, 2003.

[8] J. H. Lee, T. Tanemura, K. Kikuchi, T. Nagashima, T. Hasegawa, S. Ohara, and N. Sugimoto, "Use of 1-m Bi_2O_3 nonlinear fiber for 160-Gbit/s optical time-division demultiplexing based on polarization rotation and a wavelength shift induced by cross-phase modulation," *Opt. Lett.*, vol. 30, pp. 1267–1269, 2005.

[9] M. Scaffardi, F. Fresi, G. Meloni, A. Bogoni, L. Potı, N. Calabretta, and M. Guglielmucci, "Ultra-fast 160:10 Gbit/s time demultiplexing by four wave mixing in 1 m-long Bi_2O_3-based fiber," *Opt. Commun.*, vol. 268, pp. 38–41, 2006.

[10] M. D. Pelusi, V. G. Ta'eed, M. R. E. Lamont, S. Madden, D.-Y. Choi, B. Luther-Davies, and B. J. Eggleton, "Ultra-high nonlinear As_2S_3 planar waveguide for 160 Gb/s optical time-division demultiplexing by four-wave mixing," *IEEE Photon. Technol. Lett.*, vol. 19, no. 19, pp. 1496–1498, Oct. 2007.

[11] E. Tangdiongga, Y. Liu, H. de Waardt, G. D. Khoe, A. M. J. Koonen, H. J. S. Dorren, X. Shu, and I. Bennion, "All-optical demultiplexing of 640 to 40 Gbits/s using filtered chirp of a semiconductor optical amplifier," *Opt. Lett.*, vol. 32, pp. 835–837, 2007.

[12] K. Inoue and H. Toba, "Wavelength conversion experiment using fiber four-wave mixing," *IEEE Photon. Technol. Lett.*, vol. 4, no. 1, pp. 69–72, Jan. 1992.

[13] B.-E. Olsson, P. Ohlen, L. Rau, and D. J. Blumenthal, "A simple and robust 40-Gb/s wavelength converter using fiber cross-phase modulation and optical filtering," *IEEE Photon. Technol. Lett.*, vol. 12, no. 7, pp. 846–848, Jul. 2000.

[14] S. Nakamura, Y. Ueno, and K. Tajima, "168-Gb/s All-optical wavelength conversion with a symmetric Mach–Zehnder-type switch," *IEEE Photon. Technol. Lett.*, vol. 13, no. 10, pp. 1091–1093, Oct. 2001.

[15] J. H. Lee, Z. Yusoff, W. Belardi, M. Ibsen, T. M. Monro, and D. J. Richardson, "A tunable WDM wavelength converter based on cross-phase modulation effects in normal dispersion Holey fiber," *IEEE Photon. Technol. Lett.*, vol. 15, no. 3, pp. 437–439, Mar. 2003.

[16] K. Yamada, H. Fukuda, T. Tsuchizawa, T. Watanabe, T. Shoji, and S. Itabashi, "All-optical efficient wavelength conversion using silicon photonic wire waveguide," *IEEE Photon. Technol. Lett.*, vol. 18, no. 9, pp. 1046–1048, May 2006.

[17] V. G. Ta'eed, L. B. Fu, M. Pelusi, M. Rochette, I. C. M. Littler, D. J. Moss, and B. J. Eggleton, "Error free all optical wavelength conversion in highly nonlinear As–Se chalcogenide glass fiber," *Opt. Express*, vol. 14, pp. 10371–10376, 2006.

[18] M. R. E. Lamont, V. G. Ta'eed, M. A. F. Roelens, D. J. Moss, B. J. Eggleton, D.-Y. Choy, S. Madden, and B. Luther-Davies, "Error-free wavelength conversion via cross phase modulation in 5 cm of As_2S_3 chalcogenide glass rib waveguide," *Electron. Lett.*, vol. 43, pp. 945–947, 2007.

[19] V. G. Ta'eed, M. D. Pelusi, B. J. Eggleton, D.-Y. Choi, S. Madden, D. Bulla, and B. Luther-Davies, "Broadband wavelength conversion at 40 Gb/s using long serpentine As_2S_3 planar waveguides," *Opt. Express*, vol. 15, pp. 15047–15052, 2007.

[20] R. M. Jopson, A. H. Gnauck, and R. M. Derosier, "Compensation of fibre chromatic dispersion by spectral inversion," *Electron. Lett.*, vol. 29, pp. 576–578, 1993.

[21] S. Ayotte, S. Xu, H. Rong, O. Cohen, and M.J. Paniccia, "Dispersion compensation by optical phase conjugation in silicon waveguide," *Electron. Lett.*, vol. 43, pp. 1037–1039, 2007.
[22] J. Hansryd, P. A. Andrekson, M. Westlund, J. Li, and P.-O. Hedekvist, "Fiber-based optical parametric amplifiers and their applications," *IEEE J. Sel. Topics Quantum Electron.*, vol. 8, no. 3, pp. 508–520, May/Jun. 2002.
[23] F. Xia, L. Sekaric, and Y. Vlasov, "Ultracompact optical buffers on a silicon chip," *Nat. Photon.*, vol. 1, pp. 65–71, 2007.
[24] R. P. Webb, R. J. Manning, G. D. Maxwell, and A. J. Poustie, "40 Gb/s all-optical XOR gate based on hybrid-integrated Mach-Zehnder interferometer," *Electron. Lett.*, vol. 39, pp. 79–81, 2003.
[25] A. Bogoni, L. Potı', R. Proietti, G. Meloni, F. Ponzini, and P. Ghelfi, "Regenerative and reconfigurable all-optical logic gates for ultra-fast applications," *Electron. Lett.*, vol. 41, pp. 435–436, 2005.
[26] M. Takahashi, R. Sugizaki, J. Hiroishi, M. Tadakuma, Y. Taniguchi, and T. Yagi, "Low-loss and low-dispersion-slope highly nonlinear fibers," *J. Lightw. Technol.*, vol. 23, no. 11, pp. 3615–3624, Nov. 2005.
[27] R. E. Slusher, G. Lenz, J. Hodelin, J. Sanghera, L. B. Shaw, and I. D. Aggarwal, "Large Raman gain and nonlinear phase shifts in high-purity As_2Se_3 chalcogenide fibers," *J. Opt. Soc. Amer. B, Opt. Phy.*, vol. 21, pp. 1146–1155, 2004.
[28] T. M. Monro and H. Ebendorff-Heidepriem, "Progress in microstructured optical fibers," *Annu. Rev. Mater. Res.*, vol. 36, pp. 467–495, 2006.
[29] T. A. Birks, W. J. Wadsworth, and P. St. J. Russell, "Supercontinuum generation in tapered fibers," *Opt. Lett.*, vol. 25, pp. 1415–1417, 2000.
[30] G. Brambilla, F. Koizumi, V. Finazzi, and D. J. Richardson, "Supercontinuum generation in tapered bismuth silicate fibre," *Electron. Lett.*, vol. 41, pp. 795–797, 2005.
[31] E. C. Mägi, L. B. Fu, H. C. Nguyen, M. R. E. Lamont, D. I. Yeom, and B. J. Eggleton, "Enhanced Kerr nonlinearity in sub-wavelength diameter As_2S_3 chalcogenide fiber tapers," *Opt. Express*, vol. 15, pp. 10324–10329, 2007.
[32] Y. L. Ruan, W. T. Li, R. Jarvis, N. Madsen, A. Rode, and B. Luther-Davies, "Fabrication and characterization of low loss rib chalcogenide waveguides made by dry etching," *Opt. Express*, vol. 12, pp. 5140–5145, 2004.
[33] S. J. Madden, D.-Y. Choi, D. A. Bulla, A. V. Rode, B. Luther-Davies, V. G. Ta'eed, M. D. Pelusi, and B. J. Eggleton, "Long, low loss etched As_2S_3 chalcogenide waveguides for all-optical signal regeneration," *Opt. Express*, vol. 15, pp. 14414–14421, 2007.
[34] M. R. Lamont, C. M. D Sterke, and B. J. Eggleton, "Dispersion engineering of highly nonlinear As_2S_3 waveguides for parametric gain and wavelength conversion," *Opt. Express*, vol. 15, pp. 9458–9463, 2007.
[35] G. P. Agrawal, *Nonlinear Fiber Optics*, 3rd ed. New York: Academic, 2001.
[36] H. Takeuchi and K. Oe, "Low-loss single-mode GaAs/AlGaAs miniature optical waveguides with straight and bending structures," *J. Lightw. Technol.*, vol. 7, no. 7, pp. 1044–1054, Jul. 1989.
[37] N. Hô, J. M. Laniel, R. Vallée, and A. Villeneuve, "Photosensitivity of As_2S_3 chalcogenide thin films at 1.5 μm," *Opt. Lett.*, vol. 28, pp. 965–967, 2003.
[38] O. Aso, M. Tadakuma, and S. Namiki, "Four-wave mixing in optical fibers and its applications," *Furukawa Rev.*, vol. 19, pp. 63–68, 2000.

Mark D. Pelusi (M'00) received the B.Eng. (Hons. 1) and Ph.D. degrees in electrical engineering from the University of Melbourne, Melbourne, Vic., Australia, in 1994 and 1998, respectively.

From 1997 to 2001, he was a Research Fellow at the Femtosecond Technology Research Association, Tsukuba, Japan, where he was engaged in research on short-pulse, ultrafast optical communications. During 2001–2003, he joined Corvis Corporation, Columbia, MD, as a Senior Hardware Engineer, where he was engaged in research on broadband optical systems. Currently, he is a Research Fellow in the Centre for Ultrahigh-Bandwidth Devices for Optical Systems (CUDOS), School of Physics, University of Sydney, Sydney, N.S.W., Australia, where he is engaged in research on nonlinear optical signal processing and high-speed optical communications. His current research interests include high-speed optical communications, and nonlinear fiber-optics, and advanced waveguide devices for all-optical signal processing.

Vahid G. Ta'eed received the B.Tech. degree (with first class honors) in optoelectronics from Macquarie University, Sydney, N.S.W., Australia, in 1998. He is currently working toward the Ph.D. degree at the University of Sydney, Sydney.

He is currently a Research Associate at the Centre for Ultrahigh-Bandwidth Devices for Optical Systems (CUDOS), School of Physics, University of Sydney. He is the author or coauthor of more than 22 journal publications and 30 conference papers on topics ranging from integrated devices, nonlinear signal processing, waveguide Bragg gratings, high nonlinear chalcogenide glasses, fiber tapering, and photonics incorporating microfluidics.

Mr. Ta'eed is a member of the Optical Society of America.

Libin Fu received the Ph.D. degree in optics from Peking University, Beijing, China, in 2000.

From 2000 to 2003, he was a Postdoctoral Research Fellow with the Fiber Grating Group, Optolectronics Research Center, University of Southampton, Southampton, U.K., where he was engaged in research on novel distributed feedback laser design and high-power double-cladding fiber lasers. From April 2004 to July 2007, he was a Senior Research Associate at the University of Sydney, Sydney, N.S.W., Australia, and the Centre for Ultrahigh-Bandwidth Devices for Optical Systems (CUDOS), School of Physics, University of Sydney, where he is engaged in research on all-optical signal processing, integrated nonlinear photonic circuits, and tapering of highly nonlinear As_2Se_3 fibers. Currently, he is with IMRA America Inc., Ann Arbor, MI. His current research interests include novel continuous-wave fiber lasers, high-power short laser pulse generation and amplification, and advanced photonic devices for high-speed telecommunication systems.

Dr. Fu is a member of the IEEE Lasers and Electro-Optics Society and the Optical Society of America.

Eric Mägi received the Bachelors degree in science (honours) from the Australian National University, Canberra, Australia, in 1984, and the Ph.D. degree in mechanical engineering from the University of New South Wales, Kensington, Australia, in 1990.

From 1990 to 2000, he was with the Australia's Defence Science and Technology Organisation, as a Research Scientist/Senior Research Scientist, where he was working on fibre sensing technologies. In 1995–1996, he was with the Naval Research Laboratory, Washington, DC, as a Visiting Scientist. From 2000 to 2003, he was a Senior Instrumentations Engineer at JDS Uniphase, Australia, primarily in metrology of fibres Bragg grating devices. In 2003, he joined the Centre for Ultrahigh-bandwidth Devices for Optical Systems (CUDOS), as a Senior Research Fellow at the University of Sydney, NSW, Australia, and was responsible for the design and establishing the tapering facilities within the centre. His current research interests include nonlinear optics, design and tapering of silica, and highly nonlinear As_2Se_3 fibres for nonlinear signal processing devices.

Dr. Mägi was the recipient of the Royal Aeronautical Society Graduate Award for his Ph.D. dissertation in 1990.

Michael R. E. Lamont (S'00) received the B.Sc. degree in physics from the University of British Columbia, Vancouver, BC, Canada, in 1995, and the M.Sc. degree in physics from Simon Fraser University, Burnaby, BC, in 1999. He is currently working toward the Ph.D. degree at the Centre for Ultrahigh-Bandwidth Devices for Optical Systems (CUDOS), University of Sydney, Sydney, N.S.W., Australia.

From 2000 to 2003, he was an Optical Design Scientist at JDS Uniphase, Ottawa, ON, Canada, where he was engaged in research on tunable dispersion compensation devices using both fiber Bragg grating and multicavity etalon technologies. During 2003–2004, he joined the Medical Physics and Bioengineering Group, University College London, London, U.K., as a Chevening Technology Enterprise Scholarship Fellow, where he was engaged in research on photoacoustic imaging and commercialization of technology out of university laboratories. His current research interests include nonlinear optical signal processing, and dispersion engineering for parametric processes and supercontinuum generation in subwavelength chalcogenide planar waveguides and fiber tapers.

Steve Madden, photograph and biography not available at the time of publication.

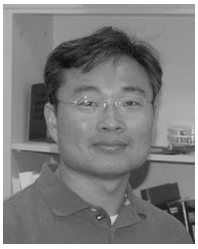

Duk-Yong Choi received the Ph.D. degree in materials science from the Department of Material Science and Engineering, Seoul National University, Seoul, Korea, in 1998.

He was a Researcher at Samsung Electronics for 6 years. Since 2005, he has been with the Centre for Ultrahigh-Bandwidth Devices for Optical Systems (CUDOS), University of Sydney, Sydney, N.S.W., Australia, where he is currently a Research Fellow. He has been engaged in the development of customized fabrication processes for realizing nonlinear optical devices based on chalcogenide glass films, and to study the structural, optical, and electrical properties of the materials. His current research interests include the characterization of novel optical materials and their fabrication into practical devices.

Douglas A. P. Bulla received the Ph.D. degree in electrical engineering from the University of Sao Paulo, Sao Paulo, Brazil, in 1999.

From 2001 to 2006, he was a Researcher at the Australian Photonics CRC, Canberra, A.C.T., Australia. In 2006, he joined the Centre for Ultrahigh-Bandwidth Devices for Optical Systems (CUDOS), University of Sydney, Sydney, N.S.W., Australia. His current research interests include chalcogenide thin film deposition for optical waveguide fabrication.

Barry Luther-Davies (SM'00) is currently a Professor and Federation Fellow at the Australian National University, Canberra, A.C.T., Australia.

He is the author or coauthor of more than 300 papers published in international journals. His current research interests include photonics, nonlinear optics, laser physics; and laser–matter interactions.

Prof. Luther-Davies is a Fellow of the Optical Society of America.

Benjamin J. Eggleton (SM'00) obtained the Bachelor's degree (with honors) in science and the Ph.D. degree in physics from the University of Sydney, Sydney, N.S.W., Australia, in 1992 and 1996, respectively.

In 1996, he joined Bell Laboratories, Lucent Technologies as a Postdoctoral Member of Staff, and was then transferred to the Department of Optical Fiber Research. In 2000, he was promoted to Research Director within the Specialty Fiber Business Division, where he was engaged in forward-looking research supporting Lucent Technologies' business in optical fiber devices. Currently, he is an ARC Federation Fellow and Professor of Physics at the University of Sydney and the Research Director of the Centre for Ultrahigh-Bandwidth Devices for Optical Systems (CUDOS), University of Sydney. He is the author or coauthor of more than 140 journal publications and numerous conference papers. His current research interests include nonlinear optics, all-optical signal processing, optical communications, photonic crystals, optofluidics, and supercontinuum.

Prof. Eggleton is a Fellow of the Optical Society of America. He was the recipient of the Malcolm McIntosh Prize for Physical Scientist of the Year at the 2004 Prime Minister's Prize for Science, the 2003 International Commission on Optics (ICO) Prize, the 1998 Adolph Lomb Medal from the Optical Society of America, the Distinguished Lecturer Award from the IEEE/Lasers and Electro-Optics Society, and the R&D100 Award. is an OSA fellow.